Economic and environmental impacts of integrating hydrogen-based technologies in the design optimization of sector-coupling energy systems in residential districts

Mohamed Eldakadosi[a] and Jana Schneeloch[b]

[a] Fraunhofer UMSICHT, Oberhausen, Germany, mohamed.eldakadosi@umsicht.fraunhofer.de (**CA**)
[b] Fraunhofer UMSICHT, Oberhausen, Germany, jana.schneeloch@umsicht.fraunhofer.de

Abstract:

Recent policies which promote climate-neutral energy systems and rising energy prices overburden the planners of energy supply systems. This leads to an increasing need for cost-effective, yet environmental-friendly, solutions. One interest-arousing approach is utilizing hydrogen-based technologies within cross-sectoral, residential energy systems. However, the economic and environmental potentials of this approach have not yet been fully uncovered. Hence, the aim of this work is to investigate the impacts of considering hydrogen-based technologies on the total costs and CO_2 emissions when designing a residential energy system. For this purpose, we developed a design optimization model using mixed-integer linear programming, whose main objective function is the minimization of total costs. The minimization of total CO_2 emissions is implemented as an epsilon constraint, where a Pareto front is created to represent optimal solutions under both objectives and their trade-off. Consequently, the optimal sizing and operation plan of the considered technologies to fulfill the energy demands of the residents are determined. Besides hydrogen-based fuel cells, electrolyzers, compressors and storage systems, the model includes photovoltaics, batteries, gas-based combined heat and power units, heat pumps, gas boilers and heat storage. For a case study of an exemplary German residential district, we carried out the design optimization for three energy systems, where two involved typical sector-coupling generation units and one included hydrogen technologies. Through the resulting Pareto fronts, we found that the energy system with hydrogen had a comparable, yet limited performance in terms of emissions reduction. However, the hydrogen system showed a poor economic competitiveness.

Keywords:

Cost Minimization, Emission Minimization, Hydrogen Systems, MILP Optimization, Sector Coupling

1. Introduction

Nowadays, planning energy systems for residential districts is facing more challenges. Decision planners must satisfy the rising energy demands while fulfilling other goals. Those goals include maintaining cost efficiency with increasing energy prices, mitigating CO_2 emissions to follow policies promoting climate-neutral energy systems, and integrating renewable energy resources with fluctuating generation. Therefore, it is becoming necessary to consider sector coupling, which describes connecting different energy sectors, such as electricity, gas and heat, while they interact with each other. Solutions to unlock the potential of sector coupling have been discussed in the literature, including electrification of heating, co-generation and power-to-gas [1–3].

Utilizing hydrogen as an energy carrier and involving it in cross-sectoral energy systems has recently attracted researchers and energy systems planners. It has been viewed as an alternative to fossil fuels and a possible storage medium for varying renewable energies. To produce and store hydrogen, electrolyzers and pressurized tanks can be used. Additionally, hydrogen can be fed to a fuel cell, which exploits electrochemical and thermodynamic hydrogen-oxygen reactions to simultaneously generate electricity and heat [4]. Solid oxide fuel cells (SOFC) and proton exchange membrane fuel cells (PEMFC) are the most installed types in residential energy systems. Nonetheless, a major drawback of hydrogen systems is their high capital and operating costs. Compared to other energy generation technologies, investing in fuel cells and electrolyzers is currently not a cost-efficient solution [5]. Another disadvantage for own hydrogen production and utilization is the low round-trip efficiency when converting electricity to hydrogen and then back to electricity [6]

Models to optimally size hydrogen-based technologies along with renewable and decentralized energy equipment have been the focus of multiple publications. For example, the authors in [7] presented a multi-objective design optimization model, using-mixed integer programming (MILP), for a multi-energy system in a neighborhood. The model included PEMFC and SOFC. While the latter could only use natural gas, the PEMFC could additionally consume hydrogen produced by a PEM electrolyzer and stored in high-pressure tanks. It has been

found that gas-based fuel cells were not optimally selected. Another optimization model to design energy hubs was introduced in [8]. It involved a fuel cell, an electrolyzer, a compressor and a refueling station. For the conducted use cases, it was not economic to install fuel cells. Another study in [9] demonstrated a developed model to optimize the sizing of an off-grid energy system for a village. The system contained a hydrogen system besides photovoltaics and batteries. The design of a similar energy system was optimized in [10], where the evolutionary algorithm and MILP were both implemented for the design and operation optimization.

We have observed that those studies focused on sizing hydrogen-based technologies as part of energy systems which also include typical generation and storage units. In most case studies, the hydrogen system was not favorable to be installed. However, it is not clear how the hydrogen systems will perform in terms of cost efficiency and emission reduction when comparing their optimal sizing and operation to typical cross-sectoral energy systems. Therefore, we created three energy systems, where a PEMFC and a PEM electrolyzer are essential elements in one of them. Using a multi-objective design optimization model, we compare the optimal solutions of the three energy systems at different points of optimal costs and emissions.

In this paper, the methodology is described in Section 2., which starts with an overview of the optimization model. Then, the objective function is presented in Section 2.2., followed by an explanation of the epsilon-constraint method in Section 2.3. Next, the model constraints are demonstrated for energy generation and storage in Section 2.4. and specifically for the hydrogen system in Section 2.5. In Section 3., the case study is illustrated. The structure of the energy systems is first clarified in Section 3.1., followed by the description of the input data in Section 3.2.. After that, the results are demonstrated in Section 3.3. and discussed in Section 3.4. Finally, Section 4. summarizes the presented work and suggests future studies as a conclusion.

2. Methodology

2.1. Overview and Implementation

To design residential energy systems under economic and environmental criteria, a multi-objective optimization model, formulated as a MILP problem, has been developed. Its aim is to minimize the total annual costs and total annual CO_2-equivalent emissions. In order to minimize two contradictory objectives, the epsilon-constraint method is utilized [11]. Simply put, the cost-minimization function is implemented as an objective function, while the emission-minimization function is applied as a constraint.

The model has been implemented using the python-based optimization package pyomo and the energy modeling package oemof-solph [12]. It provides modules that enable the modeling of various elements of an energy system. In the presented model, grids of electricity (EG) and gas (GG) are modeled by the *source* module, while the *sink* module portrays the electricity or heat demands of residential buildings. To connect different elements and ensure an energy balance, the *bus* module is added accordingly. Nevertheless, additional modules have been developed to model energy generation and storage units. In other words, decision variables and constraints describing the operation and design limits of a unit are defined inside the respective module. Those units include photovoltaics (PV), gas-based combined heat and power (G-CHP) units, battery storage (BATT), heat pumps (HP), gas boilers (GB), heat storage (HS), hydrogen fuel cell combined heat and power (FC-CHP), electrolyzers (EZ), hydrogen compressor (H2C), and hydrogen storage (H2S). This modular nature is advantageous for flexibly designing energy systems. Figure 1 provides an overview of the optimization model. It also demonstrates the inputs necessary to run the optimization model and the expected outcome of each run.

In the following subsections, a decision variable is denoted by a bold symbol, e.g., $\mathbf{P^{unit}_{out,max}}$, while a model parameter is represented by an italic symbol, e.g., $c^{unit}_{inv,a}$.

2.2. Cost-minimization function

For an optimization run, the decision variables are optimized such that the total annual costs are minimized. The objective function in (1) shows the components of the minimized costs.

$$\min : \sum_{unit} \left(\mathbf{C^{unit}_{inv,a}} + \mathbf{C^{unit}_{op,a}} \right) + \sum_{sto} \left(\mathbf{C^{sto}_{inv,a}} + \mathbf{C^{sto}_{op,a}} \right) + \sum_{grid} \left(\mathbf{C^{grid}_{imp,a}} \right) - \mathbf{R_{tot,a}} \tag{1}$$

For each unit, except for the EZ and H2C units, the annual investment cost $\mathbf{C^{unit}_{inv,a}}$ (Eur/a) is linearly dependent on the maximum output power $\mathbf{P^{unit}_{out,max}}$ (kW) as per (2). The slope of the linear function is the specific variable investment cost $c^{unit}_{inv,var,a}$ (Eur/kW/a), while the intercept is the fixed investment cost $C^{unit}_{inv,fix,a}$ (Eur/a). The latter is multiplied by the binary variable $\mathbf{y^{unit}_{inst}}$, which value decides whether the unit is installed. Regarding the annual operating cost $\mathbf{C^{unit}_{op,a}}$ (Eur/a), equation (3) includes a power-capacity-related operating cost, $c^{unit}_{op,fix,a}$ (Eur), and a variable operating cost, $c^{unit}_{op,var,a}$ (Eur/kWh), which refers to the total output power $\mathbf{P^{unit}_{out,t}}$ (kW) over all time steps t. Regarding EZ and H2C units, the specific investment and operating costs refer to the input power
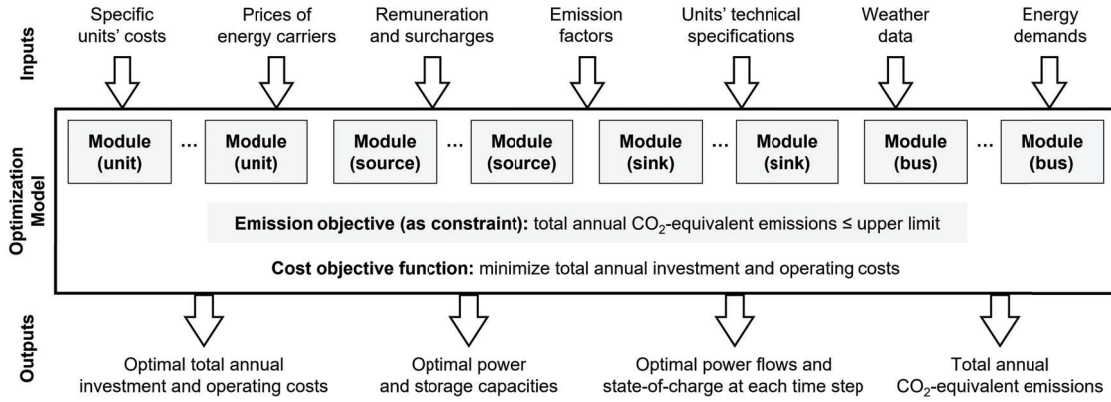
Figure 1: Overview of the developed optimization model including inputs and outputs. The optimization constraints and the decision variables are implemented accordingly in the modules.

of the unit $\mathbf{P_{in,t}^{unit}}$ (kW) or its maximum $\mathbf{P_{in,max}^{unit}}$ (kW) as demonstrated in (4) and (5). Similar to (2) and (3), the investment and operating costs for storage units (sto) are additionally considered in (6) and (7), respectively. In this case, $c_{inv,var,a}^{sto}$ (Eur/kWh/a) and $c_{op,fix,a}^{sto}$ (Eur/kWh/a) refer to the maximum usable energy capacity $\mathbf{E_{max}^{sto}}$ (kWh). Furthermore, the annual costs of importing electricity and gas from their respective grids are taken into account according to (8), where $c_{imp,t}^{EG}$ and $c_{imp,t}^{GG}$ (Eur/kWh) are the prices of electricity and gas, respectively, while $\mathbf{P_{imp,t}^{EG}}$ and $\mathbf{P_{imp,t}^{GG}}$ is the corresponding imported powers at a time step t.

$$\mathbf{C_{inv,a}^{unit}} = c_{inv,var,a}^{unit} \cdot \mathbf{P_{out,max}^{unit}} + C_{inv,fix,a}^{unit} \cdot \mathbf{y_{inst}^{unit}} \qquad \text{for } unit \notin \{EZ, H2C\} \qquad (2)$$

$$\mathbf{C_{op,a}^{unit}} = c_{op,fix,a}^{unit} \cdot \mathbf{P_{out,max}^{unit}} + c_{op,var,a}^{unit} \sum_t \left(\mathbf{P_{out,t}^{unit}} \cdot \Delta t \right) \qquad \text{for } unit \notin \{EZ, H2C\} \qquad (3)$$

$$\mathbf{C_{inv,a}^{unit}} = c_{inv,var,a}^{unit} \cdot \mathbf{P_{in,max}^{unit}} + C_{inv,fix,a}^{unit} \cdot \mathbf{y_{inst}^{unit}} \qquad \text{for } unit \in \{EZ, H2C\} \qquad (4)$$

$$\mathbf{C_{op,a}^{unit}} = c_{op,fix,a}^{unit} \cdot \mathbf{P_{in,max}^{unit}} + c_{op,var,a}^{unit} \sum_t \left(\mathbf{P_{in,t}^{unit}} \cdot \Delta t \right) \qquad \text{for } unit \in \{EZ, H2C\} \qquad (5)$$

$$\mathbf{C_{inv,a}^{sto}} = c_{inv,var,a}^{sto} \cdot \mathbf{E_{max}^{sto}} + C_{inv,fix,a}^{sto} \cdot \mathbf{y_{inst}^{sto}} \qquad (6)$$

$$\mathbf{C_{op,a}^{sto}} = c_{op,fix,a}^{sto} \cdot \mathbf{E_{max}^{sto}} \qquad (7)$$

$$\mathbf{C_{imp,a}^{grid}} = \sum_t \left(\left(c_{imp,t}^{EG} \cdot \mathbf{P_{imp,t}^{EG}} + c_{imp,t}^{GG} \cdot \mathbf{P_{imp,t}^{GG}} \right) \cdot \Delta t \right) \qquad (8)$$

Moreover, the energy system can generate annual revenues, R_a (Eur/a), by exporting excess electricity from PV and CHP units, denoted by $\mathbf{P_{exp,t}^{PV}}$ and $\mathbf{P_{exp,t}^{CHP}}$ (kW), respectively. For this case, the feed-in tariffs $r_{exp,t}^{PV}$ and $r_{exp,t}^{CHP}$ (Eur/kWh) are applied. Another source of revenues is the remuneration r_{rem}^{CHP} (Eur/kWh) for consuming a kWh of electricity from a CHP unit, symbolized by $\mathbf{P_{dem,t}^{CHP}}$ (kW), according to the CHP Act in Germany [13]. The total annual revenues are calculated as per (9).

$$\mathbf{R_{tot,a}} = \sum_t \left(\left(r_{exp}^{PV} \cdot \mathbf{P_{exp,t}^{PV}} + r_{exp}^{CHP} \cdot \mathbf{P_{exp,t}^{CHP}} + r_{rem}^{CHP} \cdot \mathbf{P_{dem,t}^{CHP}} \right) \cdot \Delta t \right) \qquad (9)$$

In this paper, the optimization horizon is one year. In order to consider investment costs of units of different lifetimes on an annual basis, they are discounted using the annuity factor as shown in (10). This factor depends on the average weighted cost of capital, *wacc*, and the lifetime of the unit, *LT* (years).

$$c_{inv,a}^{unit} = c_{inv}^{unit} \cdot \frac{wacc \cdot (1 + wacc)^{LT}}{(1 + wacc)^{LT} - 1} \qquad (10)$$

2.3. Emission minimization using the epsilon-constraint method

In Fig. 2, the steps to implement the epsilon-constraint method for emission minimization are demonstrated. The aim is to create a Pareto front that shows the trade-off between costs and emissions. In the first step, the

optimization problem is created with the decision variables and the constraints of the energy system components and the cost-minimization objective function as shown in Fig. 1. Next, the constraint in (11) is added (Step 2), which implies that the total annual emissions at the first Pareto iteration, $\varepsilon_{tot,a,1}$ (kg CO_2-equivalent/a), has no limit since it is unknown before carrying out any optimization.

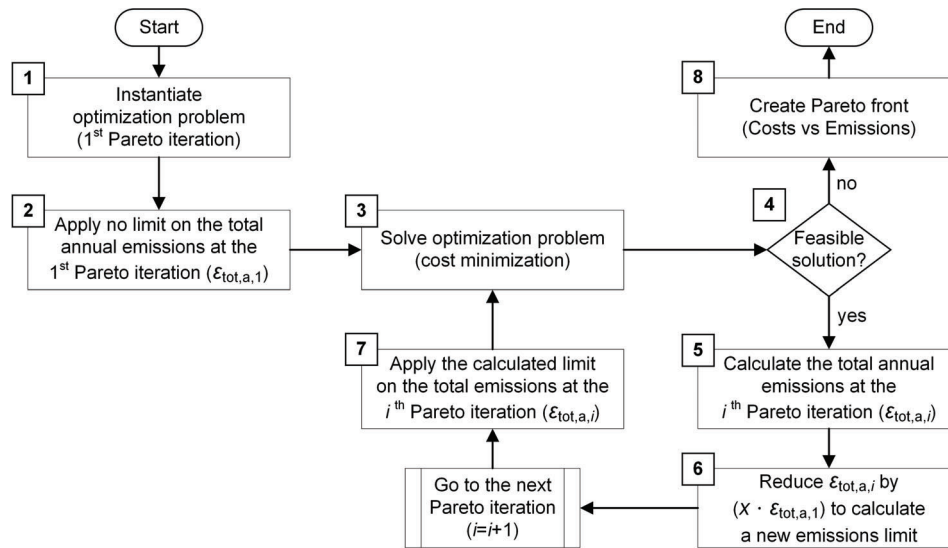$$0 \leq \varepsilon_{tot,a,1} \leq \infty \tag{11}$$

Figure 2: Process flow chart of the epsilon-constraint method.

After solving the optimization problem (Step 3), an if-statement checks whether a feasible solution has been found. If it is true, the total annual emissions at the ith Pareto iteration, $\varepsilon_{tot,a,i}$ (kg CO_2-equivalent/a), is calculated as per (12) (Step 5). It involves the amount of CO_2-equivalent emissions of the district caused by importing electricity and gas, which is determined by the respective emission factors, ε_{kWh}^{EG} and ε_{kWh}^{GG} (kg CO_2-equivalent/kWh). However, the district can reduce these emissions by exporting PV and CHP electricity to the grid, which is represented by a negative emission factor in (12), and, hence, lower the emissions in the grid. For the following Pareto iteration, a new emission limit, $\varepsilon_{tot,max,a,i+1}$, is determined by deducting a percentage x of $\varepsilon_{tot,a,1}$ from $\varepsilon_{tot,a,i}$ as per (13) (Step 6). The new limit is then applied on the total annual emissions according to (14) (Step 7). The optimization is carried out again and the loop continues until the problem has no feasible solution; i.e., the emission-optimal solution has been found. Finally, the Pareto front is created to enable the analysis of the optimal design at different points of optimal costs and emissions (Step 8).

$$\varepsilon_{tot,a,i} = \sum_t \left(\left(\varepsilon_{kWh}^{EG} \cdot \mathbf{P}_{imp,i,t}^{EG} + \varepsilon_{kWh}^{GG} \cdot \mathbf{P}_{imp,i,t}^{GG} - \varepsilon_{kWh}^{EG} \cdot \left(\mathbf{P}_{exp,i,t}^{PV} + \mathbf{P}_{CHP,i,t}^{grid} \right) \right) \cdot \Delta t \right) \tag{12}$$

$$\varepsilon_{tot,max,a,i+1} = \varepsilon_{tot,a,i} - x \cdot \varepsilon_{tot,a,1} \tag{13}$$

$$0 \leq \varepsilon_{tot,a,i} \leq \varepsilon_{tot,max,a,i} \tag{14}$$

2.4. Constraints for energy generation and storage units

Based on a unit's input power, $\mathbf{P}_{in,t}^{unit}$ (kW), and its conversion factor, CF^{unit}, its output power $\mathbf{P}_{out,t}^{unit}$ (kW) is optimized as shown in (15). For instance, the conversion factors of a CHP unit are η_{el}^{CHP} and η_{th}^{CHP}, which describe the electrical and thermal efficiencies of converting the input fuel to electricity and heat, respectively, multiplied by the lower heating value of the input fuel. Another example of a conversion factor is a heat pump's coefficient of performance (COP). In this model, the COP is calculated for each time step based on the source and flow temperatures. Furthermore, the output power cannot surpass $\mathbf{P}_{out,max}^{unit}$ as per (16). In addition, the constraint in (17) implies that $\mathbf{P}_{out,max}^{unit}$ is limited between an upper bound, $P_{max,upper}^{unit}$, and a lower bound $P_{max,lower}^{unit}$, but only if the installation of that unit is optimal; i.e., $\mathbf{y}_{inst}^{unit}$ is selected to be 1.

$$\mathbf{P^{unit}_{out,t}} = CF^{unit} \cdot \mathbf{P^{unit}_{in,t}} \tag{15}$$

$$0 \le \mathbf{P^{unit}_{out,t}} \le \mathbf{P^{unit}_{out,max}} \tag{16}$$

$$\mathbf{y^{unit}_{inst}} \cdot P^{unit}_{out,max,lower} \le \mathbf{P^{unit}_{out,max}} \le \mathbf{y^{unit}_{inst}} \cdot P^{unit}_{out,max,upper} \tag{17}$$

For a PV unit, a time series of normalized output $P^{PV}_{out,norm,t}$ (kW/kWp) is obtained using the solar irradiation and weather data of the geographical location. Based on $P^{PV}_{out,norm,t}$ and the peak power $\mathbf{P^{PV}_{out,t}}$ (kWp), the PV output $\mathbf{P^{PV}_{out,t}}$ is determined in (18). Besides the constraint in (17), $\mathbf{P^{PV}_{out,t}}$ is limited in (19) by the total available area A^{PV}_{tot} (m^2), where A^{PV}_{kWp} (m^2/kWp) is the area of a kWp PV.

$$\mathbf{P^{PV}_{out,t}} = P^{PV}_{out,norm,t} \cdot \mathbf{P^{PV}_{out,max}} \tag{18}$$

$$A^{PV}_{kWp} \cdot \mathbf{P^{PV}_{max}} \le A^{PV}_{tot} \tag{19}$$

Regarding a storage unit, equation (20) ensures the energy balance between the stored energy $\mathbf{E^{sto}_t}$ (kWh) at the current and previous time steps, along with the charging and discharging powers $\mathbf{P^{sto}_{ch,t}}$ and $\mathbf{P^{sto}_{dis,t}}$ (kW), and the respective charging efficiencies η^{sto}_{in} and η^{sto}_{out}. To represent self-discharging losses, the parameter σ^{sto}_{self} represents the percentage of energy lost per hour. The constraints in (21) to (23) represent the bounds for $\mathbf{E^{sto}_t}$, $\mathbf{P^{sto}_{ch,t}}$ and $\mathbf{P^{sto}_{dis,t}}$. In order to prevent simultaneous charging and discharging, the binary variable $\mathbf{y^{sto}_{ch,t}}$ is utilized in (24) and (25). If it is 1, then the storage unit is being charged. Similar to (17), optimizing $\mathbf{E^{sto}_{max}}$ is limited between $E^{sto}_{max,upper}$ and $E^{sto}_{max,lower}$ (kWh) with the association of $\mathbf{y^{sto}_{inst}}$.

$$\mathbf{E^{sto}_t} = \mathbf{E^{sto}_{t-1}} \cdot \left(1 - \sigma^{sto}_{self}\right) + \left(\mathbf{P^{sto}_{ch,t}} \cdot \eta^{sto}_{ch} - \mathbf{P^{sto}_{dis,t}}/\eta^{sto}_{dis}\right) \cdot \Delta t \tag{20}$$

$$0 \le \mathbf{E^{sto}_t} \le \mathbf{E^{su}_{max}} \tag{21}$$

$$0 \le \mathbf{P^{sto}_{ch,t}} \le \mathbf{P^{sto}_{max}} \tag{22}$$

$$0 \le \mathbf{P^{sto}_{dis,t}} \le \mathbf{P^{sto}_{max}} \tag{23}$$

$$0 \le \mathbf{P^{sto}_{ch,t}} \le \mathbf{y^{sto}_{ch,t}} \cdot P^{sto}_{max,upper} \tag{24}$$

$$0 \le \mathbf{P^{sto}_{dis,t}} \le \left(1 - \mathbf{y^{sto}_{ch,t}}\right) \cdot P^{sto}_{max,upper} \tag{25}$$

When connecting units, sources and sinks to each other, a bus component is included accordingly in the energy system. Its addition is equivalent to considering (26), which guarantees that the sum of all inflows equals the sum of all outflows at any time step. A special case of the bus component is the heat network (HN) module, where the inflows are multiplied by an efficiency parameter, η_{HN}, to describe distribution losses as per (27).

$$\sum_{inflow} \mathbf{P^{bus}_{inflow,t}} = \sum_{outflow} \mathbf{P^{bus}_{outflow,t}} \tag{26}$$

$$\sum_{inflow} \mathbf{P^{HN}_{inflow,t}} \cdot \eta^{HN} = \sum_{outflow} \mathbf{P^{HN}_{outflow,t}} \tag{27}$$

2.5. Constraints for hydrogen-based units

The presented constraints for hydrogen-based units are based on the work in [14], where an operation optimization model for energy systems with EZ, H2C, H2S and FC-CHP has been developed. The first component in a hydrogen system is the electrolyzer, which generates the hydrogen gas using electrical work. Equation (28) shows how the output mass flow $\mathbf{\dot{m}^{EZ}_{out,t}}$ (kg/h) is dependent on the input power $\mathbf{P^{EZ}_{in,t}}$ (kW), the standard density of hydrogen ρ_{h_2} (kg/Nm^3), and the specific energy consumption $e^{EZ}_{h_2}$ (kWh/Nm^3). Moreover, $\mathbf{P^{EZ}_{in,t}}$ is limited below $\mathbf{P^{EZ}_{max}}$ as formulated in (29). The latter is also confined in (30) by $P^{EZ}_{in,max,upper}$, $P^{EZ}_{in,max,lower}$ and $\mathbf{y^{EZ}_{inst}}$.

$$\mathbf{\dot{m}^{EZ}_{out,t}} = \mathbf{P^{EZ}_{in,t}} \cdot \rho_{h_2}/e^{EZ}_{h_2} \tag{28}$$

$$0 \le \mathbf{P^{EZ}_{in,t}} \le \mathbf{P^{EZ}_{in,max}} \tag{29}$$

$$\mathbf{y^{EZ}_{inst}} \cdot P^{EZ}_{in,max,lower} \le \mathbf{P^{EZ}_{in,max}} \le \mathbf{y^{EZ}_{inst}} \cdot P^{EZ}_{in,max,upper} \tag{30}$$

The output of the EZ unit is then fed to an H2C unit to compress the hydrogen and enable its storage in high-pressure tanks. A balance constraint, as shown in (31), is applied to the input and output mass flows. Based

on the hydrogen flow, the necessary power for compression, $\mathbf{P_{in,t}^{H2C}}$, is found in (32) using the electric efficiency η_{el}^{H2C} and the specific enthalpies at the compressor's inlet and outlet, h_{in}^{H2C} and h_{out}^{H2C} (J/kg), respectively. Both parameters depend on the pressure of the input, p_{in}^{H2C} (bar), and the output, p_{out}^{H2C} (bar), as well as the temperature at the inlet, T_{in}^{H2C} (K). The calculation is carried out using the python-based function *PropsSI* [15], which finds the value of a thermophysical property for a selected fluid by inputting the values of two other properties. Additionally, a factor of $3.6 \cdot 10^{-6}$ is used in (32) to obtain the result in kW. Constraints similar to (29) and (30) are applied to $\mathbf{P_{in,t}^{H2C}}$ and $\mathbf{P_{in,max}^{H2C}}$ with the corresponding parameters of the H2C unit.

$$\dot{m}_{in,t}^{H2C} = \dot{m}_{out,t}^{H2C} \tag{31}$$

$$\mathbf{P_{in,t}^{H2C}} = 3.6 \cdot 10^{-6} \cdot \dot{m}_{in,t}^{H2C} \cdot \left(h_{out}^{H2C} - h_{in}^{H2C} \right) / \eta_{el}^{H2C} \tag{32}$$

To identify the charging and discharging powers of the H2S unit, the average storage enthalpy h_{avg}^{H2S} (J/kg) is found using *PropsSI* by inputting the maximum and minimum storage pressures, p_{max}^{H2S} and p_{min}^{H2S} (bar), respectively, and the storage temperature T^{H2S} (K). The operating powers are then determined by (33) and (34). Analogous to (20), the stored energy E_t^{H2S} (kWh) is tracked at each time step as per (35). Further, the storage constraints (21) to (25) are applied to the energy and power variables of the H2S unit. Finally, the operation and design constraints of an FC-CHP unit are identical to the generation units' constraints in (15) to (17).

$$\mathbf{P_{in,t}^{H2S}} = 3.6 \cdot 10^{-6} \cdot \dot{m}_{in,t}^{H2S} \cdot h_{avg}^{H2S} \tag{33}$$

$$\mathbf{P_{out,t}^{H2S}} = 3.6 \cdot 10^{-6} \cdot \dot{m}_{out,t}^{H2S} \cdot h_{avg}^{H2S} \tag{34}$$

$$\mathbf{E_t^{H2S}} = \mathbf{E_{t-1}^{H2S}} + \left(\mathbf{P_{ch,t}^{H2S}} - \mathbf{P_{dis,t}^{H2S}} \right) \cdot \Delta t \tag{35}$$

3. Case Study

3.1. Structure of energy systems under investigation

To examine the hydrogen system economically and environmentally, a case study of an exemplary German residential district is conducted, where three energy systems (ES) are created. Two systems, ES 1 and 2, represent typical sector-coupling approaches. Figure 3 demonstrates the complete energy system, how the units are interconnected and which units are included in each ES. In ES 1, the primary heat supplier is a gas-CHP unit. It can also feed the electricity demand and export excess generation. In ES 2, a heat pump is solely responsible for heat generation. Finally, an FC-CHP unit is taken into account in ES 3. In this energy system, the electrolyzer produces hydrogen at 35 bar, which is then compressed to 300 bar to be stored in the hydrogen storage. In ES 1 and 3, a gas boiler is additionally considered for peak heat demands. In all systems, PV units can be installed to cover the electricity demand, supply the heat pump (in ES 2) or the electrolyzer and the compressor (in ES 3), or export the surplus energy to the grid. Besides, all energy systems can include batteries and heat storage units. The bus component *heat network* connects the central heat generation node to the demand with 5% distribution losses.

3.2. Input data

The district under study includes 13 multi-family houses with electricity and heat demands. The demand profiles were generated based on the guideline VDI 4655 [16] for one year, assuming that the total annual demands amount to 244 MWh of electricity and 1030 MWh of heat. The peak loads of both demands are 48 kW_{el} and 670 kW_{th}. The majority of the input data used, including prices of energy carriers, remunerations, surcharges and weather data, is based on the year 2020. To import electricity from the grid, a time-varying price with a mean of 0.304 Eur/kWh is applied, which is based on day-ahead prices and additional network charges and taxes [17,18]. For importing gas, a constant price of 0.076 Eur/kWh is inputted [19]. In the case of exporting PV or CHP electricity, the energy system receives revenue of 0.065 Eur/kWh [20] and 0.087 Eur/kWh [13,21], respectively. A remuneration of 0.0305 Eur/kWh is additionally awarded for the own consumption of CHP electricity [13]. Concerning the costs of technologies, linear investment functions and operating costs have been extracted from several studies and market data for PV [22], battery [9], gas CHP, gas boiler, heat pumps, heat storage [23], FC-CHP [24], electrolyzer [25], hydrogen compressor [26] and hydrogen storage [8] units. Furthermore, only emissions from importing electricity and gas from respective grids are taken into account in this study. Hence, emission factors of 0.438 [27] and 0.228 kg CO_2-equivalent [28] per kWh of imported electricity ang gas, respectively, are inputted.

A flat roof area of 4000 m^2 in total is available for the PV modules. These modules can be mounted with two different configurations: a south orientation or an east-west orientation. The available area corresponds to
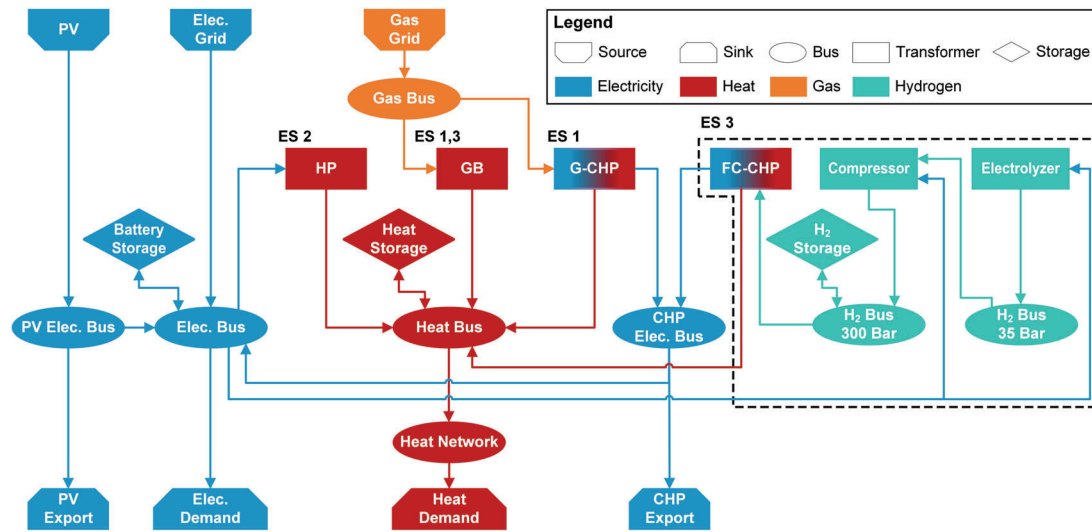
Figure 3: Complete structure of the optimized residential energy systems. Categorization of the elements follows the description in Section 2.1. The abbreviation ES implies in which energy system a unit is considered. ES 1 has a G-CHP and GB, ES 2 has only an HP, and ES 3 has a GB and hydrogen-based units.

331.5 kWp of south-oriented PV or 796 kWp of east-west-oriented PV. The PV output for each configuration, in addition to ambient temperature data, was obtained from PVGIS [29]. For the heat pump, the COP was calculated based on the given data in [30] for a flow temperature of 65 °C. The remaining technical specifications of the units are based on [4, 14, 23]. Since the gas boiler is installed to only support the main heat generator in ES 1 and 3, its sizing is limited to 400 kW.

3.3. Results

The following demonstrated results are obtained by solving the optimization problem with an hourly temporal resolution for each energy system, for multiple iterations, using the solver Gurobi [31]. Following the method presented in Section 2.3., the emission limit is reduced by $x = 5\%$ (Step 6 in Fig. 2) of the initial total annual emissions, calculated at the first Pareto iteration. Figure 4 illustrates the Pareto fronts of each energy system. Each point on the plotted curves corresponds to a solution with an optimal total annual cost for a set total annual emission. For each curve, the point on the far right portrays the cost-minimum solution (first Pareto iteration), while the far-left point represents the emission-minimum solution (last Pareto iteration). The curves also depict the best solutions in terms of costs and emissions; i.e., there are no feasible solutions with better cost-emission combinations below or to the left of the curve. For further investigation, the optimal unit sizing in terms of maximum power and maximum storage capacity is plotted for each ES in Fig. 5, while costs and emissions are demonstrated by respective categories in Fig. 6. In both figures, only selected Pareto iterations, including the first and the last, are shown for improved readability.
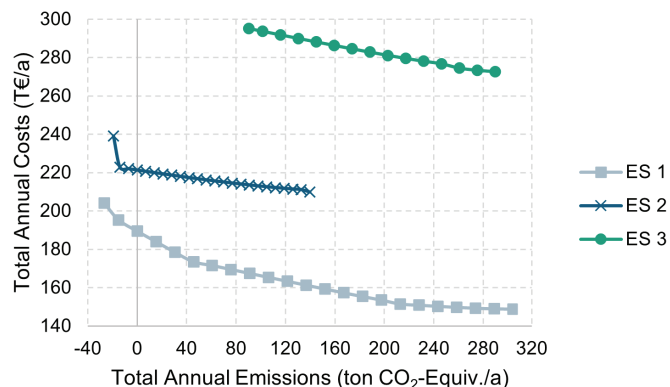

Figure 4: Pareto front (total annual costs vs. total annual emissions) of each energy system.
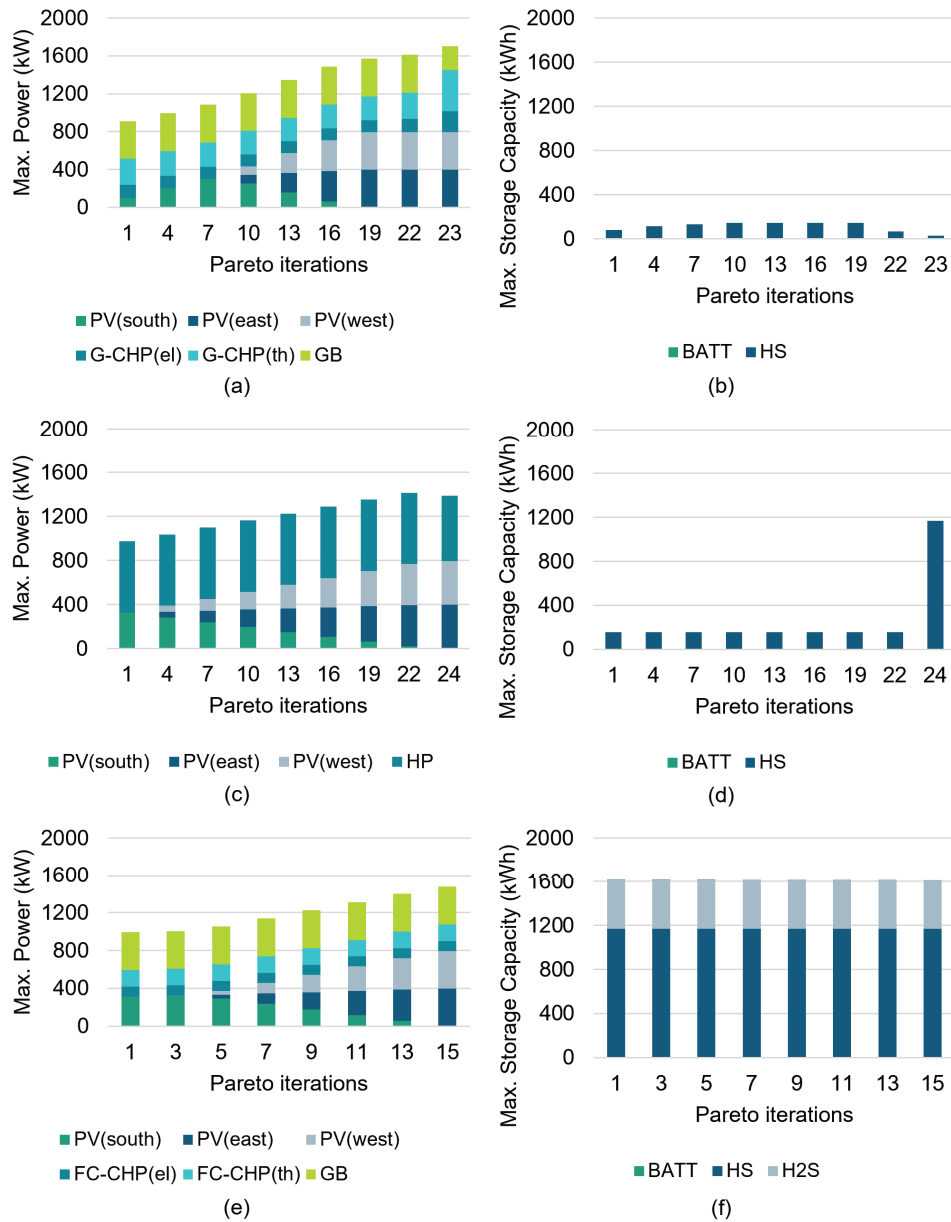
Figure 5: Optimal maximum power of generation units (a, c, e) and optimal storage capacity of storage units (b, d, f) for ES 1 (a, b), ES 2 (c, d) and ES 3 (e, f) among selected Pareto iterations. The first and last iteration corresponds to the cost optimum and the emission optimum, respectively.

3.4. Discussion

In Fig. 4, it is noticeable that the energy system with the hydrogen-based units is remarkably outperformed by the other two in terms of cost efficiency among all the Pareto iterations. In Fig. 6(e), it is evident that ES 3 has notably increased investment and operating costs in comparison to ES 1 and 2. Another observation is the comparable emission-saving performance of the hydrogen system with ES 1 and 2 for a limited number of iterations. Nevertheless, ES 1 and 2 can reduce emissions by 108% and 113%, respectively, in comparison to the first iteration. Exceeding 100% emission reduction implies that the district is producing negative emissions and, consequently, contributing to the emission mitigation in the electricity grid. On the other hand, the hydrogen system can only achieve 68%. Moreover, ES 1 economically surpasses ES 2. The main justification is that the installation of the heat pump leads to additional electricity consumption, which is more expensive than
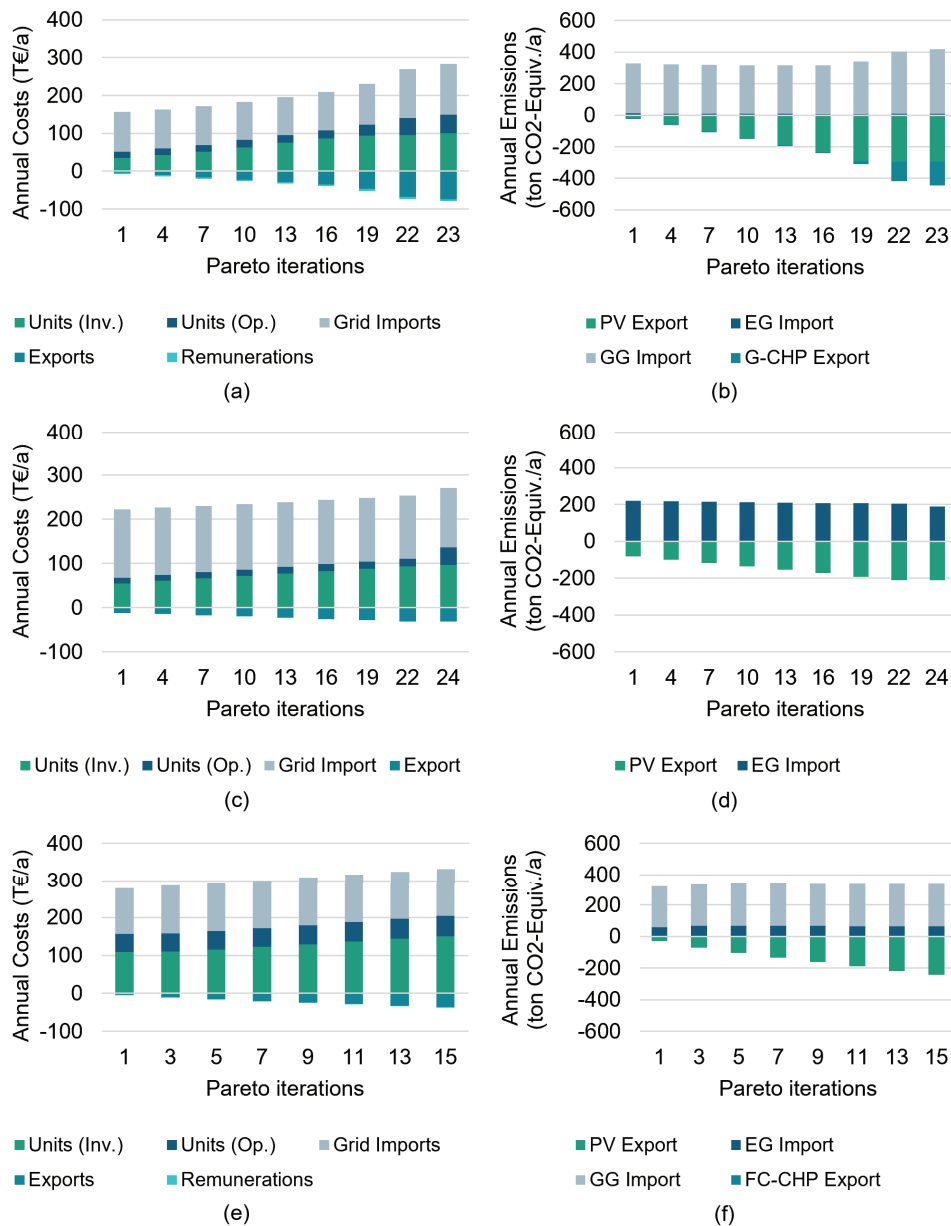
Figure 6: Optimal annual costs (a, c, e) and optimal annual emissions (b, d, f), categorized by source, for ES 1 (a, b), ES 2 (c, d) and ES 3 (e, f) among selected Pareto iterations. The first and last iteration corresponds to the cost optimum and the emission optimum, respectively.

gas, and, hence, results in higher grid import costs as shown in Fig. 6(c).

By observing the trend of reducing emissions in Fig. 4 and the resulting optimal design in Fig. 5, it can be inferred that installing additional PV peak power is the primary strategy for achieving low emission solutions for all energy systems. While lowering the emissions limit to find the emission-optimal solution, the solver attempts to first fully utilize the available area with south-oriented PV modules. After that, those modules are reduced while more east-west-oriented PV modules are recommended, since they require less area to produce the same amount of electricity as the south-oriented area, until the maximum possible peak power is reached. The primary reason is that increasing PV installation can lead to exporting more electricity to the grid and, consequently, increases the negative emissions.

Other strategies can be also noticed among the last Pareto iterations, especially after the first strategy is fully

implemented. For instance, in Fig. 5(a), the maximum power of the gas CHP unit is expanded while the sizing of the gas boiler and the heat storage is reduced in order to produce more electricity and export it to the grid. Another strategy occurs for ES 2, which is noticeable through the last iteration in Fig. 5(a) and (b). The solver recommends decreasing the heat pump's maximum power and increasing the heat storage capacity. This is accompanied by a decrease in emissions from electricity imports and fewer negative emissions from PV exports according to Fig. 6(d). This implies a rising PV supply to feed the heat pump and generate excess heat to be stored, which reduces the amount of imported electricity. However, this strategy causes comparably higher investment costs than the other iterations.

Another remark is the absence of batteries in all energy systems. A possible explanation is that in this district, exporting electricity is more economical than storing it in a battery, which requires an additional investment.

It is important to point out that the demonstrated results correspond exclusively to the input data presented in Section 3.2. Nevertheless, the drawn conclusions agree with recent literature, such as the remarks in [5] regarding the economic disadvantages of hydrogen technologies. In addition, the presented methodology with the multi-objective optimization model can be applied to other residential districts where input data are available as per described in Section 2. and illustrated in Fig. 1. Furthermore, other scenarios can lead to distinctive outcomes. For example, considering an electricity mix with a high share of renewable energy, i.e., a lower emission factor, can result in different Pareto fronts than in Fig. 4.

4. Conclusion

In this paper, we investigated the economic and environmental effects of considering hydrogen-based units on the design optimization of residential energy systems, where sector coupling could be implemented. First, a multi-objective optimization model has been developed to find the cost- and emission-optimal design and operation of different generation and storage technologies in a district, including technologies to produce and utilize hydrogen. The emission minimization has been accomplished by means of the epsilon-constraint method.

To assess the impacts of the hydrogen system, three energy systems for an exemplary district in Germany have been created. The first two involved sector coupling by gas-based co-generation and electrification through a heat pump, while the third included the hydrogen system. By comparing the respective Pareto front, it has been concluded that using hydrogen in a cross-sectoral energy system was unfavorable to obtaining competitive designs in terms of costs and emissions in comparison to typical sector-coupling approaches. It has been also determined that utilizing PV systems was a major factor in mitigating emissions.

Using the developed model, further examinations can be carried out for different energy systems structures. Another possible future work is to conduct sensitivity or scenario analysis to evaluate the performance of hydrogen systems while varying different model inputs. Moreover, further assessment criteria such as degree of self-sufficiency or self-consumption can be investigated for hydrogen systems.

Acknoweldgement

Nomenclature

Letter Symbols

C	cost, Eur
c	specific cost, Eur/kW or Eur/kWh
E	energy, kWh
h	enthalpy, J/kg
LT	life time of a unit, years
A	area, m^2
P	power, kW
p	pressure, bar
R	revenue, Eur
r	specific revenue, Eur/kWh
T	temperature, °C or K
$wacc$	weighted average cost of capital
x	reduction in emissions limit
y	binary variable

Greek symbols

Δ	difference
ε	emissions, kgCO$_2$-equiv.
η	efficiency
ρ	density, kg/m^3
σ	self-discharging losses, h^{-1}

Subscripts and superscripts

a	annual		*HS*	heat storage
avg	average		*i*	Pareto iteration
BATT	battery		*imp*	import from a grid
ch	charging		*in*	input
CHP	combined heat and power		*inst*	installation
dis	discharging		*inv*	investment
EG	electricity grid		*max*	maximum
el	electric		*norm*	normalized
exp	export to a grid		*op*	operating
EZ	electrolyzer		*out*	output
FC	fuel cell		*PV*	photovoltaics
GG	gas grid		*sto*	storage unit
grid	grid of an energy-carrier		*t*	time step
H2C	hydrogen compressor		*th*	thermal
H2S	hydrogen storage		*tot*	total
HN	heat network		*unit*	generation or storage unit

References

[1] Fridgen G, Keller R, Körner M-F, Schöpf M. *A holistic view on sector coupling*. Energy Policy 2020;147:1-8.

[2] Ramsebner J., Haas R., Ajanovic A., Wietschel M. *The sector coupling concept: A critical review*. WIREs Energy and Environment 2021;10;1:27.

[3] Sinsel SR., Riemke RL., Hoffmann VH. *Challenges and solution technologies for the integration of variable renewable energy sources—a review*. Renewable Energy 2020;145:2271–85.

[4] Ramadhani F., Hussain MA., Mokhlis H. *A Comprehensive Review and Technical Guideline for Optimal Design and Operations of Fuel Cell-Based Cogeneration Systems*. Processes 2019;7:950.

[5] Löbberding L., Madlener R. *Techno-economic analysis of micro fuel cell cogeneration and storage in Germany*. Applied Energy. 2019;235:1603–1613.

[6] DiChristopher T. *Hydrogen technology faces efficiency disadvantage in power storage race*. Available at https://www.spglobal.com/marketintelligence/en/news-insights/latest-news-headlines/hydrogen-technology-faces-efficiency-disadvantage-in-power-storage-race-65162028 [accessed 1.3.2023].

[7] Gabrielli P., Gazzani M., Martelli E., Mazzotti M. *Optimal design of multi-energy systems with seasonal storage*. Applied Energy 2018; 219:408-424.

[8] Götze J., Dancker J., Wolter M. *A general MILP based optimization framework to design Energy Hubs*. Automatisierungstechnik 2019;67:958–71.

[9] Marocco P., Ferrero D., Martelli E., Santarelli M., Lanzini A. *An MILP approach for the optimal design of renewable battery-hydrogen energy systems for off-grid insular communities*. Energy Conversion and Management 2021;245:114564.

[10] Li B., Roche R., Miraoui A. *Microgrid sizing with combined evolutionary algorithm and MILP unit commitment*. Applied Energy 2017;188:547–62.

[11] Becerra RL., Coello CAC. *Solving Hard Multiobjective Optimization Problems Using ε-Constraint with Cultured Differential Evolution*. Differential Evolution 2006;4193:543-542.

[12] oemof developer group. *oemof.solph*, Available at `https://oemof-solph.readthedocs.io/en/latest/readme.html` [accessed 14.3.2023].

[13] Heimann S. *KWK-Gesetz*. Available at `https://www.co2online.de/modernisieren-und-bauen/blockheizkraftwerk-kraft-waerme-kopplung/kwk-gesetz/` [accessed 20.2.2023].

[14] Eisenbach T. *Cross-sektoraler Einsatz von Wasserstofftechnologien - Erhebung des Stands der Technik sowie Modellierung für die wasserstoffbasierte Versorgung eines Wohnquartiers [thesis]* Bochum, Germany: Ruhr University Bochum; 2021.

[15] Maplesoft, *PropsSI*. Available at `https://www.maplesoft.com/support/help/maple/view.aspx?path=ThermophysicalData%2FCoolProp%2FPropsSI` [accessed 1.3.2023].

[16] VDI. *Reference load profiles of residential buildings for power, heat and domestic hot water as well as reference generation profiles for photovoltaic plants* Dusseldorf: Verein Deutscher Ingenieure; 2021 July.

[17] EPEX SPOT. *Market Data*. Available at `https://www.eex.com/de/marktdaten/strom/indizes` [accessed 20.1.2023].

[18] STROM-REPORT. *STROMPREISE VERGLEICHEN*. Available at `https://strom-report.de/strompreise` [accessed 10.1.2023].

[19] BDEW. *BDEW-Gaspreisanalyse Jahresbeginn 2023*. Available at `https://www.bdew.de/service/daten-und-grafiken/bdew-gaspreisanalyse/` [accessed 25.2.2023].

[20] Bundesnetzagentur. *Archivierte EEG-Vergütungssätze und Datenmeldungen*. Available at `https://www.bundesnetzagentur.de/DE/Fachthemen/ElektrizitaetundGas/ErneuerbareEnergien/ZahlenDatenInformationen/EEG_Registerdaten/ArchivDatenMeldgn/artikel.html`[accessed 4.3.2023].

[21] EEX. *Indizes*. Available at `https://www.eex.com/de/marktdaten/strom/indizes` [accessed 20.1.2023].

[22] Quaschning V. *Abschlussbericht: Beitrag der Photovoltaik zur klimaneutralen Energieversorgung im urbanen Raum (PV2City)*. Available at `https://solar.htw-berlin.de/wp-content/uploads/HTW-Abschlussbericht-PV2City.pdf`

[23] KEA-BW. *Einführung in Den Technikkatalog*. Available at `https://www.kea-bw.de/waermewende/wissensportal/technikkatalog` [accessed 1.2.2023].

[24] Wolter M., Beyrau F., Tsotsas E. *Intelligentes Multi-Energie-System(SmartMES)* Magdeburg , Germany: Otto-von-Guericke-Universität Magdeburg, Magdeburger Forum zur Elektrotechnik; 2019 Apr. `https://journals.ub.ovgu.de/index.php/MAFO/article/view/1695/1661`

[25] Smolinka T, Wiebe N, Sterchele P, Palzer A, Lehner F, Jansen M, et al. *Studie IndWEDe. Industrialisierung der Wasserelektrolyse in Deutschland*. Available at `https://www.ipa.fraunhofer.de/content/dam/ipa/de/documents/Publikationen/Studien/Studie-IndWEDe.pdf` [accessed 10.1.2023].

[26] Parks G., Boyd R. , Cornish J., Remick R. *Hydrogen Station Compression, Storage, and Dispensing Technical Status and Costs*. Available at `https://www.nrel.gov/docs/fy14osti/58564.pdf` [accessed 3.3.2023].

[27] Umwelt Bundesamt. *CO2-Emissionen pro Kilowattstunde Strom steigen 2021 wieder an*. Available at `https://www.umweltbundesamt.de/themen/co2-emissionen-pro-kilowattstunde-strom-steigen` [accessed 25.2.2023].

[28] Zukunft Gas. *Vorkettenemissionen von Erdgas*. Available at `https://gas.info/fileadmin/Public/PDF-Download/Faktenblatt-Vorkettenemission-Erdgas.pdf` [accessed 30.1.2023].

[29] European Commission. *Photovoltaic Geographical Information System (PVGIS)*. Available at `https://re.jrc.ec.europa.eu/pvg_tools/en/` [accessed 3.3.2023].

[30] WAMAK, *Heat Pump Datasheet*. Available at `https://www.wamak.eu/wapps/datasheets/v2019/datasheet.php?standard=0&fsource=A&code=WA001047&lang=en-GB.` [accessed 1.3.2023].

[31] Gurobi. *Documentation*. Available at `https://www.gurobi.com/documentation/` [accessed 1.2.2023].